

# Plasma wakefields driven by intense, broadband, incoherent electromagnetic radiation

R.M.G.M. Trines,<sup>1</sup> L.O. Silva,<sup>2</sup> J.T. Mendonça,<sup>2</sup>

W.B. Mori,<sup>3</sup> P.A. Norreys,<sup>1,4</sup> and R. Bingham<sup>1,5</sup>

<sup>1</sup>*Central Laser Facility, Rutherford Appleton*

*Laboratory, Chilton, Didcot, Oxon OX11 0QX, UK*

<sup>2</sup>*GoLP/Instituto de Plasmas e Fusão Nuclear - Laboratório  
Associado, Instituto Superior Técnico, 1049-001 Lisbon, Portugal*

<sup>3</sup>*Dept. of Physics and Astronomy, University of  
California Los Angeles, Los Angeles CA 90095-1547, USA*

<sup>4</sup>*Department of Physics, University of Oxford, Oxford OX1 3PU, UK*

<sup>5</sup>*SUPA, Department of Physics, University of  
Strathclyde, Glasgow, G4 0NG, United Kingdom*

## Abstract

Non-linear wave-driven processes in plasmas are normally described by either a monochromatic pump wave that couples to other monochromatic waves, or as a random phase wave coupling to other random phase waves. An alternative approach involves an incoherent, random or broadband pump coupling to monochromatic and/or coherent structures in the plasma. This approach can be implemented through the wave kinetic model. In this model, the incoming pump wave is described by either a bunch (for coherent waves) or a sea (for random phase waves) of quasi-particles. A particle-in-cell type code has been developed to perform numerical simulations of such interactions using the quasi-particle approach. This code allows for a comparatively easy description of both random phase and coherent pump pulses coupling to slow electrostatic plasma waves, while providing an extended range of powerful diagnostics leading to a deeper physical insight into the dynamics of the fast waves. As an example, the propagation of short, intense laser pulses through a plasma has been simulated. A sample of the phenomena that can be studied for this case includes modulational instabilities, photon wave breaking and turbulence, and pulse compression, stretching, and chirping. The extensibility of the numerical implementation to other types of fast wave-slow wave interactions is also discussed.

## INTRODUCTION

It is a well-known fact that in the numerical modelling of plasma physics, the plasma particles can be described as if they were a fluid. Fluid codes, Vlasov codes, and magneto-hydrodynamic codes are all based on this observation. The fact that in the interaction of fast, short-wavelength waves with a plasma, the fast wave modes can actually be described as a bunch of particles is less known. However, in the case that there is a clear separation in time and length scales between populations of “fast” and “slow” waves in the plasma, it may be worthwhile to regard the ensemble of fast modes as a distribution of quasi-particles. This approach to wave-plasma interaction is commonly called *wave kinetics* [1]. Tappert and Besieris [2] identified the power of the Wigner-Moyal [3, 4] formalism to study classical wave equations using phase space distribution functions. The field is represented by a Wigner distribution of quasi-particles (photons, plasmons etc), and in the limit of short wavelengths the transport equation is formally equivalent to the Vlasov equation. An analogy between particle dynamics and field dynamics can then be easily established, leading to new and revealing physical insight. A similar formalism has been developed in solid state physics to describe phonon interactions [5], while the Wigner-Moyal formalism has also been used to study electromagnetic wave propagation in random media in the geometrical optics approximation [6]. It has been successfully used in the study of weak turbulence in plasmas since the 1960’s [7] and more recently in the study of photon Landau damping [8] and ultra-intense laser-plasma interactions [9]. The Vlasov-like structure of the photon kinetic equation provides the ideal setting to examine photon dynamics under the particle-in-cell (PIC) framework [2, 10, 11]. The most powerful features of the photon kinetic code is its simplicity and the natural way in which broadband and angular spread effects can be included in the formalism.

The concept of wave-kinetics has been developed initially to study the interaction of electromagnetic (EM) waves with plasmas, e.g. in laser wakefield acceleration, but has meanwhile been extended to other areas of plasma physics as well [8, 9, 12–14]. At its heart lies the *wave action*  $N(t, x, k)$  of the incoming pump wave, which is defined as  $N(t, x, k) = W(t, x, k)/\omega(k)$ . Here,  $W$  denotes the energy density of the wave as a function of time, position, and wave number (i.e. momentum of the wave mode), and  $\omega(k)$  is the wave mode frequency as given by the linear dispersion relation. Since the energy of a wave

mode comes in quanta of size  $\hbar\omega(k)$ , the quantity  $N$  is a measure of the density of wave quanta or *quasi-particles* for each wave number  $k$ . Owing to the fact that wave action is, in general, a conserved quantity [15], the evolution of  $N(t, x, k)$  is then governed by a Vlasov-type equation, of which the factors  $dx/dt$  and  $dk/dt$  are provided by a pair of Hamiltonian equations of motion, also known as the paraxial-ray or ray-tracing equations. The specific approach allows one to follow the propagation of a broad spectrum of wave modes simultaneously, as opposed to conventional approaches that allow only a limited number of modes to be followed in a single simulation.

A range of complex phenomena can be investigated using the wave-kinetic approach that cannot be studied by other means. These include: photon acceleration and deceleration, Landau-like damping of plasma waves by photons, photon wave breaking and turbulence, broadband modulational instabilities, and stretching/steepening of short laser pulses. Applications in laser-plasma interaction are many, such as wakefield excitation, broadband laser-plasma interaction (e.g. induced spatial incoherence), strong plasma turbulence (e.g. the Langmuir wave collapse), and so on. There may also be numerous applications in other areas involving the interaction of a broad spectrum of fast waves with a plasma.

The code described in this paper solves the Vlasov equation for the wave action  $N(t, x, k)$  using the well-known particle-in-cell (PIC) method [10, 11]. There are only two other known attempts to write such a code: one by Tappert et al. [16], who did not include the plasma response to the EM waves in their model, and one by Silva et al. [9], who used a quasi-static model for the plasma response. To our knowledge, this code is the first to use a fully non-linear, relativistic, non-quasi-static model for the plasma response. As the particles involved are (quasi-)photons in our case, we have decided to call it a photon-in-cell code. This code has been used to simulate the propagation of a short, intense laser pulse through a slab of underdense plasma. The particle model for the photons has been coupled to a cold-fluid model for the plasma. Even though this model is rather basic, the code produces quite remarkable results. If necessary, the fluid model can be replaced with more advanced models (PIC or Vlasov) for the plasma evolution. Some basic features of the code: it is less computationally demanding than a full PIC code, provides a much simpler description of the EM waves than the “slowly evolving envelope” approximation, gives better physical insight into the EM field dynamics than most existing codes, and allows for an easy description of broadband, incoherent light pulses.

This paper is organized as follows. In Section 2, a description of the theory of wave kinetics, in particular photon kinetics, is given. Section 3 contains a detailed description of the numerical code we have developed to based on the wave-kinetic model. Section 4 contains several examples of typical applications of the code. These serve to demonstrate the capabilities of the code, as well as the advanced diagnostics that it provides, which give a deeper insight into the physics underlying the simulation results than can be obtained with many commonly used simulation techniques. Finally, Section 5 contains the conclusions that can be drawn from the presented results, as well as an overview of the ways in which the code can be extended and/or improved.

## THEORETICAL BACKGROUND

The theoretical foundation for the quasi-particle approach consists of three main parts: the Wigner-Moyal description of classical EM fields and the associated Vlasov-like equation describing the conservation of quasi-particles, the dispersion relation for the quasi-particles and the associated kinetic equations, and the ponderomotive force exerted by the quasi-particles on the plasma. We will treat these briefly.

The Wigner-Moyal formalism for the description of waves, which is well-known from quantum-mechanical theory, can also be employed to describe the propagation of classical EM fields [17, 18]. In the framework of this formalism, the equation describing wave propagation through a dispersive medium (i.e. a plasma) assumes the familiar Vlasov-like description when the fields evolve on a much faster time scale than the medium, and quantities like the susceptibility  $\chi$  evolve on the same slow time scale as the medium. The central quantity in the Wigner-Moyal description is the quasi-particle density  $N(t, x, k)$ , given by  $N(t, x, k) = W(t, x, k)/\omega(k)$ , where  $W(t, x, k)$  is the energy density of the Fourier component of the field with wave number  $k$  at time  $t$  and position  $x$ . For a given EM field  $\vec{E}(t, x)$ , the corresponding quasi-particle density is obtained using the Wigner function:

$$F(t, x, k) = \int E(t, x + s/2) \cdot E^*(t, x - s/2) \exp(-iks) ds \quad (1)$$

from which  $N(t, x, k)$  can be derived as follows:

$$N(t, x, k) = \frac{\epsilon_0}{8\hbar} \left( \frac{\partial D}{\partial \omega} \right)_{\omega(k)} \cdot F(t, x, k). \quad (2)$$

Here,  $D = 0$  is the dispersion relation of the medium in which the quasi-particles are propagating, and  $\omega(k)$  is derived from the same dispersion relation. From  $N$ , both the square of the electric field and its vector potential can be derived quickly:

$$E^2(t, x) = \frac{\hbar}{\epsilon_0} \int \frac{dk}{(2\pi)^3} \omega(k) N(t, x, k), \quad A^2(t, x) = \frac{\hbar}{\epsilon_0} \int \frac{dk}{(2\pi)^3} N(t, x, k) / \omega(k).$$

The quasi-particle density  $N$  obeys the following equation:

$$\frac{dN}{dt} = \frac{\partial N}{\partial t} + \frac{dx}{dt} \frac{\partial N}{\partial x} + \frac{dk}{dt} \frac{\partial N}{\partial k} = S(t, x, k, N), \quad (3)$$

where the source term  $S$  contains slow variations of the refractive index  $\epsilon$  of the medium, as well as terms governing the creation and absorption of quasi-particles. For a broad range of applications, these contributions can be neglected, i.e.  $S \approx 0$ , and (3) reduces to the Liouville equation for the quasi-particle density  $N$ .

When there is a clear separation between fast and slow time scales, the propagation of radiation through a medium is mostly governed by the corresponding linear dispersion relation. For example, for EM radiation propagating through a plasma, we have  $D = \omega^2 - \omega_p^2(x, t)/\gamma - c^2 k^2 = 0$ , where  $\omega_p$  denotes the local electron plasma frequency, and  $\gamma$  is the relativistic mass correction factor. From this dispersion relation, a relation of the form  $\omega = \omega(k)$  can be derived, e.g.  $\omega(k) = \sqrt{\omega_p^2(x, t)/\gamma + c^2 k^2}$ . Taking into account that  $\omega(k)$  serves as the effective Hamiltonian for the canonical ray equations, we derive the factors  $dx/dt$  and  $dk/dt$  in (3) from the well-known ray tracing equations:

$$\frac{dx}{dt} = -\frac{\partial D / \partial k}{\partial D / \partial \omega} = \frac{\partial \omega}{\partial k}, \quad \frac{dk}{dt} = \frac{\partial D / \partial x}{\partial D / \partial \omega} = -\frac{\partial \omega}{\partial x}. \quad \frac{d\omega}{dt} = -\frac{\partial D / \partial t}{\partial D / \partial \omega} = \frac{\partial \omega}{\partial t} \quad (4)$$

These equations allow one to describe the full evolution of the quasi-particle density  $N(t, x, k)$  in a plasma of given density. Numerical implementation can be realized by means of e.g. a Vlasov or a particle-in-cell code; the latter approach will be explored in this paper.

The third topic we need to address here is the action of the quasi-particles on the medium. Together with the evolution equation for  $N$ , knowledge of this action will allow us to produce a self-consistent description of the interaction between the radiation and the medium through which it propagates. The action is given by the ponderomotive pressure  $F_p(x, t)$  *per unit volume*, as found in [19]:

$$F_p(x, t) = g_{sq} \int \frac{dk}{(2\pi)^3} N(t, x, k) \nabla H_{\text{eff}} - g_{sq} \int \frac{dk}{(2\pi)^3} \nabla \left[ N(t, x, k) \frac{\partial H_{\text{eff}}}{\partial n_{bg}} n_{bg} \right],$$

where  $g_{sq}$  is the quasi-particle statistical weight (accounts for spin degeneracy of the QPs),  $H_{\text{eff}}$  is the effective Hamiltonian for the canonical ray equations, and  $n_{bg}$  is the background density of the medium. For photons propagating through a plasma with background density  $n_0$ , we have  $H_{\text{eff}} = \omega(k) = \sqrt{\omega_p^2(x, t)/\gamma + c^2 k^2}$ , and

$$F_p(x, t) = -\frac{\omega_{pe}^2}{2\gamma} g_{ph} \nabla \int \frac{dk}{(2\pi)^3} N(t, x, k)/\omega(k). \quad (5)$$

where  $g_{ph}=1$  ( $g_{ph}=2$ ) for circular (linear) polarization, and  $n_0$  denotes the background plasma electron density. For a plane EM wave  $(\omega_0, k_0)$ , the QP density is given by  $N = |E_0|^2/(8g_{ph}\pi\hbar\omega_0)\delta(k - k_0)$ , and the ponderomotive force *acting on a single electron* takes the more familiar form ( $A^2$  denotes the wave's vector potential):

$$F_p(x, t) = -\frac{e^2}{2m_e\gamma} \nabla A^2,$$

Together with a model for the evolution of the plasma electrons, the equations (2), (3), (4) and (5) allow us to describe the propagation of an arbitrary laser pulse in an underdense plasma in a self-consistent manner. In the next section, we will describe the numerical implementation of these equations that we have developed.

## THE PHOTON-IN-CELL ALGORITHM

### Description of the algorithm

The photon-in-cell algorithm is based on the fact that the equation for the evolution of the quasi-particle density (3) is nothing different from the well-known Vlasov equation for the evolution of the plasma electron or ion density. Thus, a number of proven techniques are available to us for the numerical study of that equation. We have chosen to employ the so-called particle-in-cell method. This method makes full use of the fact that the quasi-particle number density  $N$  is conserved along the flow lines in quasi-particle phase space. In other words, if  $N$  is the superposition of a certain number of  $\delta$ -distributions at  $t = 0$ , i.e.  $N(0, x, k) = \sum_i \delta(x - x_i(0))\delta(k - k_i(0))$ , then the Vlasov equation (3) guarantees that  $N$  will remain the superposition of the same number of  $\delta$ -distributions for all time, and one only has to keep track of the locations  $(x_i(t), k_i(t))$  of the distributions in phase space. This evolution is governed by the characteristics of the Vlasov equation:

$$\frac{dx_i}{dt} = \frac{\partial \omega}{\partial k}(t, x_i(t), k_i(t)), \quad \frac{dk_i}{dt} = -\frac{\partial \omega}{\partial x}(t, x_i(t), k_i(t)),$$

where  $\omega(t, x, k)$  is provided by the dispersion relation for the quasi-particles under consideration. (See below.)

For the plasma electrons, we have employed a 1-dimensional cold fluid model. The model is fully non-linear and relativistic, as linear and weakly non-linear models yielded unsatisfactory results. The ions are treated as a static background. First we apply the following scaling to our equations:  $t \rightarrow \omega_p t$ ,  $x \rightarrow \omega_p x/c$ ,  $\omega \rightarrow \omega/\omega_p$ ,  $k \rightarrow ck/\omega_p$ ,  $p \rightarrow p/(m_e c)$ ,  $n \rightarrow n/n_0$ ,  $E \rightarrow eE/(m_e \omega_p c)$ ,  $A \rightarrow eA/(m_e c)$ . Here,  $n_0$  is the plasma background density,  $\omega_p = (e^2 n_0 / (\epsilon_0 m_e))^{1/2}$  denotes the corresponding plasma frequency, and other symbols have their usual meaning. The scaled equations then read:

$$\frac{\partial n}{\partial t} + \frac{\partial}{\partial x} \left( \frac{np}{\gamma} \right) = 0, \quad (6)$$

$$\frac{\partial p}{\partial t} + \frac{p}{\gamma} \frac{\partial p}{\partial x} = -E - \frac{1}{2\gamma} \frac{\partial A^2}{\partial x}, \quad (7)$$

$$A^2 = \int \frac{dk}{(2\pi)^3} \frac{N(t, x, k)}{\omega(k)}, \quad (8)$$

$$\frac{\partial E}{\partial x} = 1 - n. \quad (9)$$

For a circularly polarized laser pulse, we have  $\gamma = \sqrt{1 + p^2 + A^2}$ , and the evolution equation for  $p$  simplifies to

$$\frac{\partial p}{\partial t} + \frac{\partial \gamma}{\partial x} = -E. \quad (10)$$

For the scaled dispersion relation, we now find

$$\omega(t, x, k) = \sqrt{n / \sqrt{1 + p^2 + a^2} + k^2},$$

from which we find the equations of motion for the photons:

$$\frac{dx_i}{dt} = \frac{k_i}{\omega(t, x_i, k_i)}, \quad \frac{dk_i}{dt} = -\frac{1}{2\omega(t, x_i, k_i)} \frac{\partial}{\partial x} \left( \frac{n}{\gamma} \right). \quad (11)$$

The equations (6), (10) and (11), together with the equations for  $E$ ,  $A^2$ ,  $\gamma$  and  $\omega$ , form a closed system for the evolution of the combined radiation-plasma system. We have created a numerical implementation of this scheme based on the following steps:

1. Create a grid spanning the simulation box; quantities like  $n$ ,  $p$ , and  $A^2$  will be known on this grid;
2. For a given laser pulse, initialize the photon number density using (1) and (2);

3. Load the quasi-particles in such a way that their distribution matches the number density calculated in the previous step; project them onto the grid to obtain  $A^2$ ;
4. Initialize  $n$ ,  $p$ , and other field quantities;
5. Advance  $n$  and  $p$ ;
6. Advance  $x_i$  and  $k_i$  for all quasi-particles;
7. Advance all other field quantities;
8. Project the photons onto the grid to obtain the new value of  $A^2$ .

The steps 5-8 are repeated for each time cycle.

There are a number of practical issues arising during the implementation of the above scheme. These will be discussed in the next subsection.

### Implementation

The practical implementation of the above scheme consists of three distinct parts: initialization, field and particle advance, and particle projection. Each will be treated here briefly.

**Initialization.** The initialization stage works as follows. First, a monospaced grid is created. On this grid, the plasma electron density is initialized to the (prescribed) value of the background ion density, while the plasma fluid momentum is initialized to zero, so the plasma is initially neutral and stationary. Then for each grid cell, the (prescribed) quasi-particle density is integrated over all  $k$  values to determine the total number of quasi-particles for that cell. Next the quasi-particles are loaded for each cell; the positions are allocated deterministically, while the wave numbers are allocated randomly. This way, the effective quasi-particle density corresponds to an approximation of the prescribed one that is piecewise linear in the  $x$ -direction and piecewise constant in the  $k$ -direction. Once they are loaded, the particles are projected onto the grid to determine  $A^2$ . This is not a straightforward procedure: to calculate  $A^2$  one needs  $\omega(k_i)$  for each particle, to calculate  $\omega(k_i)$  one needs the Lorentz factor  $\gamma(x_i)$ , and to calculate  $\gamma(x_i)$  one needs  $A^2$  again. To overcome this problem, we set  $\gamma = 1$  everywhere, and then alternatingly project the photons and recalculate  $\gamma$ .



Eventually this process leads to a converging value for  $A^2$ ; for our case, it was sufficient to repeat the procedure twice.

**Field and particle advance.** For the advancement of both fields and particles, we resort to a second-order Runge-Kutta scheme. While this is a straightforward procedure for the canonical quasi-particle equations, the applicability of this scheme to the fluid equations is not immediately apparent. We recall that the 1-D fluid equations read:

$$\frac{\partial n}{\partial t} = -\frac{\partial}{\partial x} \left( \frac{np}{\gamma} \right), \quad \frac{\partial p}{\partial t} = -E - \frac{\partial \gamma}{\partial x}.$$

By discretizing the right-hand side of these equations, to get rid of the  $x$ -derivatives, we get:

$$\begin{aligned} \frac{\partial n}{\partial t} &= \frac{-1}{2h} ((np/\gamma)(x+h) - (np/\gamma)(x-h)), \\ \frac{\partial p}{\partial t} &= \frac{-1}{2h} (E(x+h) - E(x-h) + \gamma(x+h) - \gamma(x-h)). \end{aligned} \tag{12}$$

If we then advance  $n$  and  $p$  across the whole grid at once, instead of node-by-node, the equations (12) can be treated as ordinary differential equations, to which the Runge-Kutta scheme can be applied as usual.

In order to properly implement the Runge-Kutta scheme, we have to keep track of a number of auxiliary quantities; apart from  $n$  and  $p$ , intermediate values for  $E$ ,  $\gamma$ ,  $n/\gamma$ ,  $\partial/\partial x(n/\gamma)$ , and  $np/\gamma$  are used.

The Runge-Kutta scheme roughly works as follows:

1. Advance  $n$ ,  $p$ ,  $x$ ,  $k$  for  $0.5 * \delta t$ ;
2. Update  $\gamma$  using intermediate values for  $p$  but old values for  $A^2$ ;
3. Project photons to obtain intermediate value of  $A^2$
4. Update  $\gamma$  and all other derived field quantities;
5. Advance  $n$ ,  $p$ ,  $x$ ,  $k$  for  $\delta t$ , using the intermediate values for all quantities calculated before;
6. Update  $\gamma$  using new values for  $p$  but intermediate values for  $A^2$ ;
7. Project photons to obtain new value of  $A^2$

8. Update  $\gamma$  and all other derived field quantities;

Although this scheme is not the most efficient in terms of memory use, its benefits are clear. The scheme is very stable and tolerates solutions that are strongly non-linear. Peak values of  $n/n_0 = 10$  have been reached, i.e. very close to wave breaking, before the simulation would become unstable and break down.

**Projection.** We have used quadratic splines to accumulate the contributions of the particles to  $A^2$  onto the grid, as well as to interpolate field quantities, which are only known on grid nodes, at the positions of the particles. Although a quadratic spline is more expensive computationally than a linear one, the use of quadratic splines leads to significant noise reduction and solutions that are more stable, especially for long runs. The following spline function has been used:

$$f(x) = \begin{cases} 0.75 - x^2, & |x| < 0.5, \\ 0.5 * (1.5 - |x|)^2, & 0.5 \leq |x| < 1.5, \\ 0, & |x| \geq 1.5. \end{cases}$$

This function is continuous with a continuous first derivative, and satisfies  $f(x-1) + f(x) + f(x+1) = 1$  for  $|x| < 0.5$ . The latter property ensures proper photon number density conservation.

After the photons have been projected and  $A^2$  has been obtained, a four-pass binomial filter is applied to the result. This has been found to be necessary to suppress numerical instabilities that otherwise grow uncontrollably and destroy the result in the long run. These instabilities result from modulational instabilities (which do not have a well-determined wave length, unlike parametric instabilities) are growing from any kind of numerical noise around. Fortunately, the instabilities occur at (much) shorter wave lengths than the interesting physics, which allows one to filter them out as long as the grid is not too coarse. The use of a compensation filter turned out to be undesirable, as it would undo the effect of the filter on the instabilities.

It should be noted that additional filtering cannot be used as a substitute for the use of quadratic splines. This is due to the fact that filtering has shown to be very effective on fast-growing instabilities, but less so on slow-growing instabilities that might show up during (very) long runs. The latter kind is much more effectively suppressed by using quadratic splines instead of linear ones.

## APPLICATIONS

To demonstrate the possibilities of the photon-kinetic approach, and to benchmark the code, we have used it to simulate the interaction of laser pulses having various lengths with a slab of cold, underdense plasma. The pulses have a Gaussian-shaped envelope, and as they are taken to be coherent, their spectral bandwidth is inversely proportional to their length. Their peak intensity is given by  $a_0 = 0.7$ .

The plasma slab has a constant background density, which is scaled to 1. The degree to which the plasma (plasma frequency  $\omega_p$ ) is underdense with respect to the laser pulse (mean wave number  $k_0$ ) is fully determined by the parameter  $ck_0/\omega_p$ . We will therefore characterize our simulations by the value of this parameter rather than individual values of  $\omega_p$  and  $k_0$ .

We shall treat two different cases: a “long” pulse (having an FWHM of several times  $c/\omega_p$ ) and a “short” pulse (having an FWHM that is less than  $c/\omega_p$ ). The observed interaction is quite different from one case to the next, and we will show that the photon kinetic approach is well suited to explore these differences. We will also demonstrate the wide range of new diagnostics that come with this approach.

### Long pulse

The interaction of a long pulse (FWHM  $\approx 24c/\omega_p$ , i.e. some 4 plasma wavelengths) with an underdense plasma is dominated by the modulational instability. This is caused by the fact that  $\nabla A^2$  is too small initially to drive a significant wakefield. However, the nature of the photon equations of motion (11) is such, that photons tend to clump together at slight density depressions of the plasma fluid. Conversely, the ponderomotive force of a clump of photons tends to push the plasma away, so wherever the photon density is slightly raised, the plasma density will be depressed, and vice versa. Even the smallest ripples in either the plasma density or the pulse envelope will be amplified and develop into a plasma wave with frequency  $\sim \omega_p$  and a speed comparable to that of the driving laser pulse, i.e.  $\sim (1 - (1 - (ck_0/\omega_p)^2)^{-1})^{1/2}$ .

A simulation of a long pulse traversing the plasma has been conducted, the results of which are displayed in Figure 1. The pulse has an FWHM of about  $24c/\omega_p$ , and a mean wave number  $k_0 = 7.0 * \omega_p/c$ . The spread in wave numbers is Fourier-matched to the pulse length,

in order to have a coherent pulse. Snapshots of photon  $(x, k)$ -space, the plasma electron density, as well as the envelope of the pulse's vector potential, taken at various times, are displayed. There is a vast spectrum of interesting phenomena that can be observed here. First of all, there is photon acceleration/deceleration, which comes in two flavours: change of  $k$  for constant  $\omega$ , and change of  $\omega$  for constant  $k$ . The first case corresponds to a photon moving through a plasma of which the density is constant in time, and corresponds to optical refraction in a dispersive medium. The second case corresponds to a photon moving through a plasma of which the density is (locally) constant in space, but not in time. This type of interaction leads to energy transfer between the photons and the plasma, and also to a change in colour of the photons. Initially, there is mostly energy transfer from the photons to the plasma, for the creation of the plasma wave. However, energy may also flow in the opposite direction, in which case the photons are gaining energy and doing a blue shift at the expense of the plasma wave.

When there is simultaneous acceleration and deceleration of particles, there is always a good chance of exciting turbulence. This is no different for quasi-particles. Quasi-particle turbulence works as follows. In the case of an unchirped laser pulse, the mean value of  $k$  is constant through the pulse initially. When the modulational instability is triggered, there will not only be a modulation on the spatial distribution of the quasi-particles, but also on their mean  $k$ -value, and thus on their (group) velocity. When the simulation progresses, this modulation increases in amplitude, until such time that fast quasi-particles from the back of the pulse start to overtake slow quasi-particles from the front. This actually constitutes “wave breaking” of the quasi-particle wave. Meanwhile, a significant plasma wave has been created, and most quasi-particles will be trapped in the troughs of this wave. Fast particles moving to the front of a trough will be decelerated by the increasing plasma density, move to the back of the trough, will be accelerated by the increasing plasma density they meet there, and move to the front again. In quasi-particle  $(x, k)$ -space (phase space), one observes groups of quasi-particles, each group confined to its own trough, revolving around an O-point.

By this time, the plasma density fluctuations are driven far into the non-linear regime, even if one started out with a pulse intensity that is still in the linear regime. The reason for this is, that the pulse envelope has been modulated on the length scale of the plasma wave, and thus exhibits peaks spaced  $c/\omega_p$  apart. This can clearly be seen in the plots on the right of Figure 1. Note that the red curve follows the actual profile of  $|A|^2$ , while the

black curve denotes the original profile for reference. The peaks in  $|A|^2$  lead to large values for  $\nabla A^2$ , i.e. for the associated ponderomotive force, far in excess of the values obtained from the shallow slopes of the original envelope. As they are also spaced approximately one plasma wavelength apart, they act in resonance with the plasma wave itself, and drive it much more efficiently and to much larger amplitudes than an unmodulated pulse ever would. When a wakefield is excited by a long pulse through the mechanism we just described, it is commonly called *self-modulated* laser wakefield excitation [20].

### Short pulse

The interaction of a short pulse (FWHM  $\approx 1.8 * c/\omega_p$ , i.e. about 0.3 plasma wavelength) with the plasma is dominated by photon deceleration and the transfer of energy from the photons to the plasma. For the case of a reasonably underdense plasma, the pulse velocity will be close to  $c$ , and the wave buckets will be approximately  $c/\omega_p$  in length, i.e. longer than the pulse itself. For this reason, the photons will mostly be grouped at the front of the first wave bucket, and there will be neither photon acceleration nor turbulence. Also, the modulational instability is not expected to occur.

A simulation has been conducted, the results of which are displayed in Figure 2. The pulse has an FWHM of about  $1.8c/\omega_p$ , and a mean wave number  $k_0 = 14.0 * \omega_p/c$ . Again, the spread in wave numbers is Fourier-matched to the pulse length. In the figure, as in Figure 1, graphs of the photon phase space and  $n/n_0$  are shown on the left, while the evolution of the pulse's envelope is shown on the right. At the start of the interaction, we observe that the pulse excites a wakefield, and that the photons lose energy and momentum in the process. It is interesting to note that the photons right after the centre of the pulse lose the most energy. This follows from the fact that  $d\omega/dt = \partial\omega/\partial t = (1/2\omega)\partial n/\partial t$ , and  $\partial n/\partial t$  is most negative directly behind the pulse centre. The photons at the the pulse's extremities find themselves in regions where  $|\partial n/\partial t|$  is small, and hardly see any energy change. This leads to a characteristic V-shape of the photons in phase space.

Looking at the evolution of the pulse envelope, i.e.  $|A|^2$ , we find that it initially steepens while its peak value increases. This is a direct consequence of the decrease of  $\omega$  for the particles at the centre of the pulse. As  $|A_k|^2 = N_k/\omega_k$ , and  $N_k$  is conserved, any decrease in  $\omega_k$  will initially lead to an increase in  $|A|^2$ . Only after the photons are spread out along

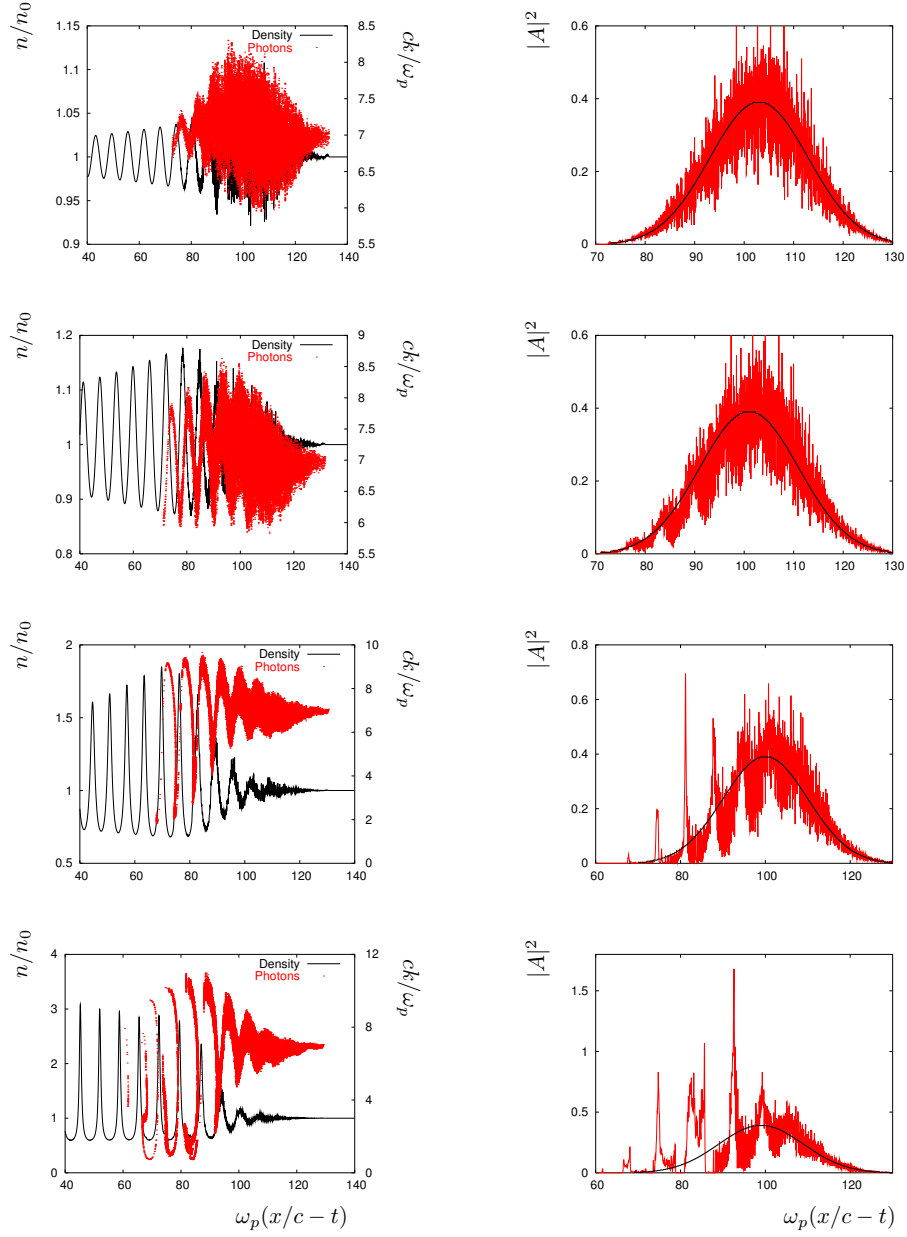


Figure 1: Simulation results for the long pulse (FWHM  $\approx 24*c/\omega_p$ ) at (a)  $\omega_p t = 250$ , (b)  $\omega_p t = 375$ , (c)  $\omega_p t = 500$ , and (d)  $\omega_p t = 625$ . The graph on the left shows  $n/n_0$  (black curve, left scale) and photon momentum  $ck/\omega_p$  (red dots, right scale) versus position  $\omega_p(x/c - t)$ . The growth of the modulational instability, as well as photon confinement and turbulence, are clearly present. The graph on the right shows  $|A|^2$  for the pulse (red curve). The peaks at the back of the pulse give evidence of the modulational instability. The black curve depicts the original pulse profile for reference.

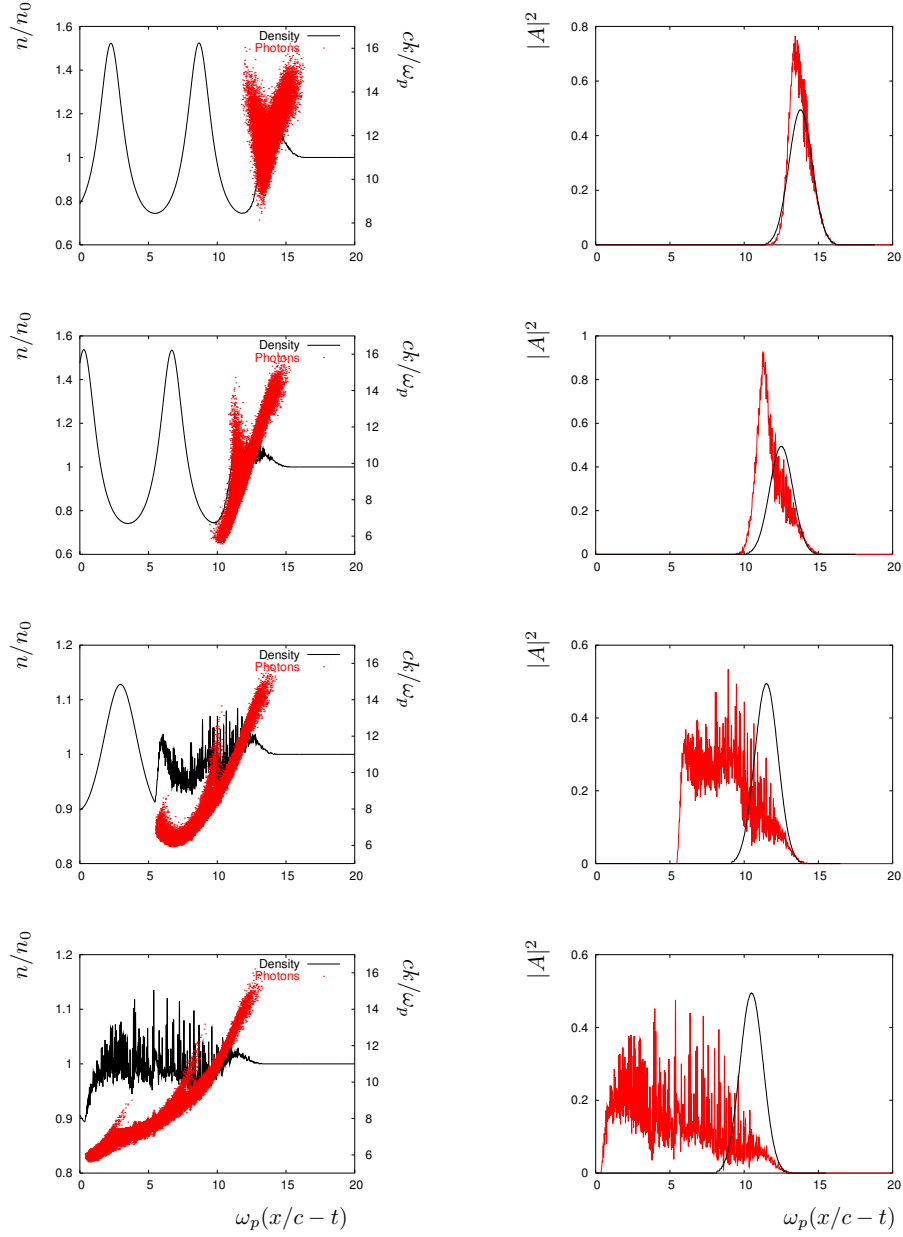


Figure 2: Simulation results for the short pulse (FWHM  $\approx 1.8 * c/\omega_p$ ) at (a)  $\omega_p t = 467$ , (b)  $\omega_p t = 933$ , (c)  $\omega_p t = 1400$ , and (d)  $\omega_p t = 1867$ . The graph on the left shows  $n/n_0$  (black curve, left scale) and photon momentum  $ck/\omega_p$  (red dots, right scale) versus position  $\omega_p(x/c - t)$ . It is obvious that photons in the middle of the pulse lose much more energy than those at the ends, resulting in stretching and chirping of the pulse. The graph on the right shows  $|A|^2$  for the pulse (red curve). One observes initial pulse compression and steepening, whereas the pulse is stretched and flattened at later times. The black curve depicts the original pulse profile for reference.

a larger length, will the peak amplitude of the vector potential decrease. See also Tsung *et al.* [21] for a detailed description of this effect.

As the interaction progresses, the slowest photons (low  $k$ -value) will start to lag behind with respect to the fastest photons. This will cause the pulse to be stretched and chirped (i.e. tilted in phase space). Due to the continued energy transfer from the photons to the plasma, the mean values of  $\omega$  and  $k$  for the pulse as a whole will decrease, causing it to undergo a general redshift. We also find that the pulse (moving with  $v_g < c$ ) is lagging behind with respect to the simulation box (moving with  $c$ ), and more so for decreasing photon momentum.

At even later times, a clump of photons that were at the centre of the pulse originally, has lost so much energy and is lagging so far behind, that they now form the back of the pulse. These photons are now encountering a region of increasing plasma density at the back of the first wave bucket, causing their momentum and energy to increase once more, at the expense of the wakefield. This might eventually lead to photon turbulence, as in the case of the long pulse with modulational instability, if it weren't for the fact that the pulse, already having spent most of its energy, is no longer able to generate a wakefield of sufficient intensity for this. Eventually, these photons will escape from the first wave bucket, leading to further stretching of the pulse and depletion of its energy.

This particular simulation provides new insights into the internal dynamics of a short, intense laser pulse driving a wakefield. It shows us which part of the pulse is driving the wake, and also provides a more thorough picture into the chirping, stretching and flattening of the pulse that occurs when the pulse loses a significant amount of its energy to the wakefield. Such knowledge can be used, for example, to tailor laser pulses in order to increase the efficiency with which they drive the wakefield.

## CONCLUSIONS

In this paper, we have investigated the wave kinetic approach as a novel way to study non-linear wave-plasma interactions. We have shown that this approach is particularly suitable in the case of a random phase pump wave interacting with coherent structures in the plasma, while its extended set of available diagnostics provides a deeper insight into the turbulent dynamics of the fast wave modes.



We have developed and tested a PIC-type code to implement the photon-kinetic model for the interaction of EM waves with an underdense plasma. In doing so, we have identified the important issues in the development and operation of such a code. First of all, one needs to choose a proper model for the plasma response. The linear model we tried first proved to be much too limited for the applications we had in mind, and introduced additional noise into the simulation as well. The non-linear relativistic model we are using today serves well for a range of applications. Second, the proper projection of the particles onto the grid. Even though it may be tempting to use a linear spline because it is fast and easy to use, our results show that a quadratic spline performs better especially for longer runs, and is to be preferred. Finally, there is the issue of filtering. As with most particle codes, our code suffers from noise; it has however been found that the growth of noise can be kept under control by proper filtering of the (square of the) vector potential. However, this does not lead to a complete obliteration of the noise, and we may have to resort to other measures to achieve that goal.

The code has been tested on the interaction of laser pulses with a slab of underdense plasma. The pulse has been represented by quasi-photons, while a fluid model has been employed for the plasma. Two cases have been investigated: a “long” pulse (several plasma periods in length) and a “short” pulse (shorter than a single plasma period). For the long pulse, we have observed the following phenomena: photon acceleration/deceleration, photon “wave breaking,” photon turbulence, and modulational instabilities. For the short pulse we have found the following phenomena: initial pulse compression and steepening, selective energy transfer to the plasma wave (photons at the centre lose most, photons at both ends hardly affected), and pulse chirping, stretching and flattening at later times.

The photon kinetic treatment offers new diagnostics that provide a deeper insight into the dynamics of wave-plasma interaction than available with present-day codes that treat the EM waves as coherent fields. The simulation results reveal a complex interaction structure that remains hidden otherwise. This is one of the strong points of the wave kinetic approach.

The deeper insight into pulse dynamics can be employed to tailor pulses to produce a wakefield with some desired properties more effectively. As systems to deliver tailor-made laser pulses are becoming more and more available, numerical simulations to accompany the experimental results will soon be badly needed. The photon kinetic method can supply the demand.

There is a number of issues that deserve further investigation. First of all, the code should be generalized to two and three dimensions. This is a necessary step, as most other codes in the field employ at least two spatial dimensions. Also, given the speed of current computers and the expected improvements, there is no reason not to do this. Second, we need better ways to deal with the noise responsible for short-wavelength modulational instabilities should be found. We can fight the symptoms using filtering, but digging out the root cause is the better option in the long run, especially since we may wish to apply the wave-kinetic approach to other types of wave-plasma interaction. Third, we wish to extend the the wave-kinetic approach, and in particular its numerical implementation, to other types of fast wave-slow wave interactions. Restricting ourselves to photons will not do the method justice. There are already many proven codes in the field to deal with the problem of laser-plasma interaction. Whereas this renders benchmarking of our code easier, it also means that there is not much territory left to cover in that direction. However, there exist many other turbulent wave-plasma interactions for which no suitable numerical model has been developed so far, such as interactions between fast and slow plasma waves in a magnetized plasma. Such waves occur in a vast range of different situations, but no numerical methods to attack them efficiently have been developed to date. However, now that we have demonstrated the wave-kinetic method successfully, its application to a wide spectrum of turbulent wave-plasma interactions lies within reach.

- 
- [1] Sagdeev, R. Z. and Galeev, A. A., *Nonlinear Plasma Theory* (Benjamin, New York, 1969).
  - [2] Besieris, I.M. and Tappert, F.D., *J. Math. Phys.***14**, 704, (1973).
  - [3] Wigner, E., *Phys. Rev.* **40**, 749 (1932).
  - [4] Moyal, J.E., *Proc. Camb. Phil. Soc.* **45**, 99, (1949).
  - [5] Peierls, R.E., *Quqntum Theory of Solids* (Oxford University Press, Oxford, 1995).
  - [6] McDonald, S.W., *Phys. Rep.* **158**, 337, (1988).
  - [7] Kadomtsev, B.B., *Plasma Turbulence* (Academic Press, London, 1965).
  - [8] R. Bingham *et al.*, *Phys. Rev. Lett.* **78**, 247 (1997).
  - [9] L.O. Silva *et al.*, *IEEE Trans. Plas. Sci.* **28**, 1202 (2000).
  - [10] J. M. Dawson, *Rev. Mod. Phys.* **55**, 403-447 (1983).

- [11] C. K. Birdsall and A. B. Langdon, *Plasma Physics via Computer Simulation* (Institute of Physics Publishing, Bristol and Philadelphia, 1991).
- [12] R. Bingham *et al.*, Physics Letters A **220**, 107 (1996).
- [13] L. O. Silva and J. T. Mendonça, Phys. Rev. E **57**, 3423 (1998).
- [14] J. T. Mendonça, R. Bingham, P. K. Shukla, Phys. Rev. E **68**, 0164406 (2003).
- [15] G. B. Whitham, *Linear and Nonlinear Waves* (John Wiley & Sons, New York, 1974).
- [16] F. D. Tappert, W. J. Cole, R. H. Hardin and N. J. Zabusky, in *Proceedings of the Fourth Conference on Numerical Simulation of Plasmas, 1970, Washington, D.C.*, edited by J. Boris and R. Shanny (Office of Naval Research, Arlington, VA, 1971), 196.
- [17] F. D. Tappert, SIAM Rev. (Chronicle), **13**, 281 (1971).
- [18] J. T. Mendonça, *Theory of Photon Acceleration*, Series in Plasma Physics (Institute of Physics Publishing, Bristol and Philadelphia, 2001).
- [19] L. O. Silva, R. Bingham, J. M. Dawson, and W. B. Mori, Phys. Rev. E **59**, 2273 (1999).
- [20] E. Esarey, P. Sprangle, J. Krall, and A. Ting, IEEE Trans. Plas. Sci. **24**, 252 (1996), and references therein.
- [21] Tsung *et al.*, Proc. Nat. Ac. Sci. USA **99** (1), 29-32 (2002).